ACS OMEGA

Open Access

This article is licensed under CC-BY-NC-ND 4.0

http://pubs.acs.org/journal/acsodf

Article

Simulation of Fixed-Bed Chromatographic Processes Considering the Nonlinear Adsorption Isotherms

Ambreen Khan* and Shamsul Qamar

Cite This: *ACS Omega* 2023, 8, 38301−38312

Read Online

ACCESS | Metrics & More | Article Recommendations

ABSTRACT: This paper presents the numerical approximation of a nonlinear equilibrium-dispersive (ED) model of multicomponent mixtures for simulating single-column chromatographic processes. Using Danckwerts boundary conditions (DBCs), the ED is studied for both generalized and standard bi-Langmuir adsorption isotherms. Advection−diffusion partial differential equations are used to represent fixed-bed chromatographic processes. As the diffusion term is significantly weaker than the advection term, sophisticated numerical techniques must be applied for solving such model equations. In this study, the model equations are numerically solved by using the Runge−Kutta discontinuous Galerkin (RKDG) finite element method. The technique is designed to handle sudden changes (sharp discontinuities) in solutions and to produce highly accurate results. The method is tested with several case studies considering different parameters, and its results are compared with the high-resolution finite volume scheme. One-, two-, and three-component liquid chromatography elutions on fixed beds are among the case studies being considered. The dynamic model and its accompanying numerical case studies provide the initial step toward continuous monitoring, troubleshooting, and effectively controlling the chromatographic processes.

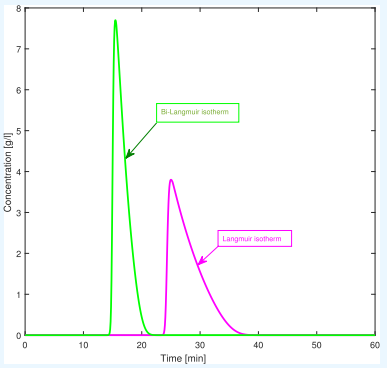

INTRODUCTION

Chromatography is a commonly used technique for identifying, separating, and purifying the components of a mixture for a qualitative and quantitative examination. It is used to perform many complicated separations in laboratories and industries. In the pharmaceutical industry, chromatography is utilized to identify unknown substances and to ensure the purity of mixtures; in the food industry, it is used to measure the nutrient content of products, and in the chemical sector, it is used to examine samples of water and to monitor the quality of air. It is also employed in other industries, including the petroleum industry, biotechnology, and biochemical processes, as well as fingerprinting, forensic science, protein separation like plasma fractionation, and insulin and enzyme purification.[1−4]

In chromatography, a part of the molecules of a compound is adsorbed on the stationary phase, while the other fraction is in the mobile phase. A constant and relatively fast exchange of the molecules between the two phases results in an effective velocity of the molecule distribution lower than the velocity of the mobile phase. The interactions of the molecules of different compounds with the stationary phase are different, resulting in different effective velocities and separation. The rate at which the components elute from the stationary phase depends on their physical and chemical properties, such as their size, shape, and affinities for the stationary phase. The mixture components that interact strongly with the stationary phase travel slowly as compared to those which have weak interaction with the stationary phase. This allows the components to be separated and identified based on their unique properties. Chromatography includes a variety of techniques, such as gas chromatography, liquid chromatography, and thin-layer chromatography, each with its own advantages and disadvantages and suited for different types of mixtures and applications.

The literature has discussed the process of mass transfer and separation in chromatographic columns through the use of various mathematical models with differing levels of complexity. Several models have been developed to describe the transport of solutes in porous media. These include the equilibrium-dispersive (ED) model, the lumped kinetic model, and the general rate model.[2−4] Each of these models is built as a set of partial differential equations (PDEs) of the convection−diffusion type along with additional differential or algebraic equations to supplement the model. The adsorption isotherm associated with these models determines their linearity and nonlinearity. Convection-related practical problems appear in a variety of applications, including weather

Received: June 30, 2023
Accepted: September 21, 2023
Published: October 3, 2023

ACS Publications

© 2023 The Authors. Published by American Chemical Society

forecasting, gas dynamics, oceanography, meteorology, oil recovery simulation, granular flows, turbulent flows, modeling of shallow waters, contaminant transport in porous media, viscoelastic flows, magnetohydrodynamics, semiconductor device simulation, electromagnetism, and many more. In this paper, the nonlinear ED model considering the bi-Langmuir adsorption isotherm is utilized. The analytical solution is not feasible. Consequently, the only method for finding a solution is to use a precise, reliable, and effective numerical technique. In general, the finite difference (FD), finite element method (FEM), and finite volume method (FVM) are three well-known numerical techniques that can simulate chromatographic processes.[3,5,8,9,12−16,44] These techniques are widely recognized and well-established methods for numerical simulations. The FD is based on the discretization of the spatial domain into a grid of discrete points and the approximation of the partial derivatives in the governing equations. The FEM involves the discretization of the spatial domain into a set of interconnected elements and the approximation of the partial derivatives by using shape functions. The FVM is based on the discretization of the spatial domain into a set of control volumes, each of which represents a portion of the fluid in the chromatography column. Each of these numerical techniques has its own strengths and limitations. In this article, we used discontinuous Galerkin (DG) FEM as a numerical technique because of its diversity, flexibility, and stability, which is well suited for convection-dominated problems.

DG Method. The DG method is a numerical technique for approximating PDE solutions. Unlike traditional FEMs, the DG method allows for the use of piecewise polynomial basis functions that are discontinuous at element interfaces. This provides more flexibility in terms of mesh geometry and the choice of basis functions, making the DG well-suited for solving complex and heterogeneous problems. The DG method has a wide range of applications, including the simulation of fluid flows, electromagnetic fields, acoustics, and structural mechanics. It has also been used in astrophysics, climate science, materials science, and among other fields. The neutron transport equation, a linear hyperbolic equation for a scalar-valued variable, was first tackled numerically by Reed and Hill who devised the first DG method in 1973.[6] The importance of the method was recognized by Lesaint and Raviart who performed its initial theoretical analysis in 1974.[7] Over the time, the DG method has undergone gradual development as it was applied to a variety of problems, ultimately leading to its successful extension to nonlinear unsteady hyperbolic systems by Cockburn and Shu in the 1990s.[36,37] Since then, the method has seen an incredibly rapid development. In this paper, we employ a high-order Runge−Kutta DG (RKDG) method. In arbitrary order, DG schemes usually offer higher accuracy for general chromatography settings as demonstrated in previous studies. However, it has been shown recently that there are chromatography settings where unstabilized arbitrary order methods may struggle in chromatography settings with strong gradients.[43] Nonoscillatory schemes can be more efficient and prevent negative values, which can have considerable amplitude for the standard DG methods.[35] Hence, we choose a stabilized/TVD DG scheme that is limited to second-order but retains stability for such settings. The method combines the features of the Runge−Kutta method and the DG method to produce an accurate and efficient solution for the given model equations.

Paper Organization. The content of the paper is as follows. The one-dimensional nonlinear ED is first discussed, and then the proposed numerical method (RKDG) is deduced for a single-component ED model. After that, there is a discussion on the considered numerical test problems, and in the end, conclusions are provided.

Nonlinear ED Model. This paper centers on the ED model, which enables the anticipation of solute particle distribution along the column, encompassing the retention time and peak shape of each solute. The ED model rests on five primary assumptions, which are outlined below.[11]

1 The chromatographic process is isothermal which means temperature remains constant.
2 The column is homogeneous both along its radii and in the angular direction.
3 The solid phase of the column is occupied by a porous material composed of spherical particles with a uniform size. This material acts as a filter for the substances that are being separated in the column and plays an essential role in the separation process.
4 The liquid phase is incompressible.
5 The process has axial dispersion, which generates band broadening of the concentration profiles.

Additionally, an apparent dispersion coefficient $D_{\mathrm{app},k}$ is introduced by adding together all mass transfer limitations imposed on axial dispersion and nonequilibrium isotherms. The one-dimensional mass balance equation for the ED model is expressed as

$$\frac{\partial C_k}{\partial t} + F\frac{\partial q_k^*}{\partial t} + u\frac{\partial C_k}{\partial z} - D_{\mathrm{app},k}\frac{\partial^2 C_k}{\partial z^2} = 0, \quad \text{for } k = 1, 2, \ldots N_{\mathrm{C}} \tag{1}$$

The variable N_{C} symbolizes the sample's number of components. The solute concentration of the kth component in the mobile and stationary phases is represented by $C_k(t, z)$ and $q_k^*(t, z)$, respectively. The linear mobile phase velocity is represented by u, while the axial coordinate is denoted by z and the time coordinate is represented by t. The phase ratio is given by $F = (1 - \epsilon)/\epsilon$, where ϵ is the total porosity of the column packing.

Adsorption Isotherm. The equilibrium adsorption isotherms explain the solute distribution in a chromatography column between the liquid and solid phases. Since the nature of interactions differs from system to system, various adsorption isotherm models have been constructed and are presented in the literature. They are classified as linear, Langmuir, BET, Freundlich isotherm, and many others.[3,4,23] Here, the nonlinear bi-Langmuir isotherm is taken into account. This isotherm is used to describe the adsorption of molecules onto a surface. It is a combination of the Langmuir and BET isotherms and assumes that adsorption occurs in two separate layers, with a monolayer forming first, followed by a multilayer. The bi-Langmuir model can provide more accurate predictions of adsorption behavior than either the Langmuir or BET models alone, especially when there is a high degree of surface heterogeneity. The parameters in the bi-Langmuir equation can be determined experimentally and used to compare the adsorption properties of the different materials. The model has a wide range of applications, including in environmental remediation, food science, and pharmaceuticals.

https://doi.org/10.1021/acsomega.3c04641
ACS Omega 2023, 8, 38301−38312

For the N-component mixture, the competitive bi-Langmuir isotherm is expressed as

$$q_k^*(C) = \frac{a_{k\mathrm{I}} C_k}{1 + \sum_{j=1}^{N_C} p_j b_{j\mathrm{I}} C_j} + \frac{a_{k\mathrm{II}} C_k}{1 + \sum_{j=1}^{N_C} p_j b_{j\mathrm{II}} C_j},$$
$$k = 1,2,3, \ldots, N_C \tag{2}$$

where the coefficients a_k represent Henry's constant for the k-th component in the mixture, while b_k quantifies the nonlinearity of the isotherm. The terms p_j in the denominator can have either positive or negative signs, enabling the mixture to exhibit either Langmuir or anti-Langmuir behavior, as described in[24,25] The subscripts I and II refer to two distinct adsorption sites.

The model eq 1 is subjected to the appropriate initial and boundary conditions (BCs).

Initial Conditions. The expressions for the initial conditions (ICs) are as follows

$$C_k(t = 0, z) = C_{k,\mathrm{in}}, \qquad q_k(t = 0, z) = q_{k,\mathrm{in}}^*,$$
$$k = 1, 2, 3, ..., N_C \tag{3}$$

Boundary Conditions. We consider the standard Danckwerts BCs at the column inlet and evaluate a rectangular injection profile.[26] For k-th component $C_{k,\mathrm{inj}}$ is injected concentration, and BC at the inflow end of the column is defined as

$$C_k(t, z = 0) - \frac{D_{\mathrm{app},k}}{u}\frac{\partial C_k(t, z = 0)}{\partial z} = \begin{cases} 0, & \text{if } t > t_{\mathrm{inj}} \\ C_{k,\mathrm{inj}}, & \text{if } 0 \le t \le t_{\mathrm{inj}} \end{cases} \tag{4}$$

Finally, the outflow conditions at the column outlet $z = L$ are given below

$$\frac{\partial C_k(t, z = L)}{\partial z} = 0, \qquad \forall\, t \ge 0 \tag{5}$$

The injected concentration of the k-th component is denoted by $C_{k,\mathrm{inj}}$, and the injection time is symbolized as t_{inj}.

NUMERICAL SCHEME

The proposed model, as represented by eq 1, is solved numerically by using the total variation-bounded Runge−Kutta DG (TVB-RKDG).[33,34] To derive the numerical scheme, we first convert the second-order system to a first-order system and obtain the weak formulation. Then the DG scheme will be used in a spatial coordinate that transformed the provided PDEs into a system of an ODE in time, and then an explicit and nonlinearly stable high-order Runge−Kutta method, i.e., TVB-RK, is applied to solve the resulting ODE system. Here, a single-component ED model with $N_C = 1$ and $C_k = C$ is used for the derivation of the numerical scheme. Thus, we get

$$\frac{\partial C}{\partial t} + F\frac{\partial q^*}{\partial t} + u\frac{\partial C}{\partial z} - D_{\mathrm{app}}\frac{\partial^2 C}{\partial z^2} = 0 \tag{6}$$

or

$$\frac{\partial}{\partial t}(C + Fq^*(C)) + \frac{\partial}{\partial z}\left(uC - D_{\mathrm{app}}\frac{\partial C}{\partial z}\right) = 0 \tag{7}$$

and define

$$f(C, g) = uC - \sqrt{D_{\mathrm{app}}}\, g(C),$$
$$w(C) = C + Fq^*(C) \tag{8}$$

where $g(C) = \sqrt{D_{\mathrm{app}}}\frac{\partial C}{\partial z}$ as invented by Bassi and Rebay.[10] After substituting eq 8 in eq 7 we get a system of PDEs as given below

$$\frac{\partial w}{\partial t} = -\frac{\partial f}{\partial z} \tag{9}$$

$$g(C) = \sqrt{D_{\mathrm{app}}}\frac{\partial C}{\partial z} \tag{10}$$

Space Discretization. The spatial variable z is discretized for $l = 1, 2, ..., N_z$, each mesh interval has a constant width Δz, the cell partitions and domain of the cell l are $z_{l+1/2}$ and $\Omega_l = (z_{l-1/2}, z_{l+1/2})$, respectively. The width of the cell l is $\Delta z_l = z_{l+1/2} - z_{l-1/2}$ and $\Omega = U\Omega_l$ is the portion of the whole domain. Let $w_a(t, z)$ be the approximate solution to $w(t, z)$ for each time $t \in [0, T]$ in finite dimensional space

$$V_a = \{v \in L^1(\Omega): v|_{\Omega_l} \in P^p(\Omega_l), \qquad l = 1,2, \ldots, N_z\} \tag{11}$$

The collection of polynomials having degrees p that are defined over the cell Ω_l is $P^p(\Omega_l)$. To obtain an approximation of solution $w_a(t, z)$, we need to derive a weak formulation. This can be achieved by multiplying eqs 9 and 10 with a smooth function $v(z) \in L^2(\Omega_l)$ and integrating by parts over the interval Ω_l, leading to the following expression

$$\int_{\Omega_l}\frac{\partial w}{\partial t}v(z)\mathrm{d}z = -\left(f\left(C_{l+\frac{1}{2}}, g_{l+\frac{1}{2}}\right)v\left(z_{l+\frac{1}{2}}\right) - f\left(C_{l-\frac{1}{2}}, g_{l-\frac{1}{2}}\right)v\left(z_{l-\frac{1}{2}}\right)\right) + \int_{\Omega_l}\left(f(C, g)\frac{\partial v(z)}{\partial z}\right)\mathrm{d}z \tag{12}$$

$$\int_{\Omega_l} g(C)v(z)\mathrm{d}z = \sqrt{D_{\mathrm{app}}}\left(C_{l+\frac{1}{2}}v\left(z_{l+\frac{1}{2}}\right) - C_{l-\frac{1}{2}}v\left(z_{l-\frac{1}{2}}\right)\right) - \sqrt{D_{\mathrm{app}}}\int_{\Omega_l} C(z)\frac{\partial v(z)}{\partial z}\mathrm{d}z \tag{13}$$

Here, $P_m(z)$, the Legendre polynomials of order m, are used as local basis functions to apply eq 11. The property of L^2-orthogonality of Legendre polynomials can be utilized, that is

$$\int_{-1}^{1} P_m(s)P_n(s)\mathrm{d}s = \left(\frac{2}{2m + 1}\right)\delta_{mn} \tag{14}$$

For each $z \in \Omega_l$, the approximate solutions w_a and g_a belongs to the finite dimensional space V_a and can be written as

$$w_a(t, z) = \sum_{m=0}^{p} w_l^{(m)}\phi_m(z),\ g_a(C_a(t, z)) = \sum_{m=0}^{p} g_l^{(m)}\phi_m(z) \tag{15}$$

$$\phi_m(z) = P_m\left(\frac{2(z - z_l)}{\Delta z_l}\right), \qquad m = 0,1, \ldots, p \tag{16}$$

Here, linear basis functions are used; therefore, $m = 0, 1$. By using eqs 14−16, we get

https://doi.org/10.1021/acsomega.3c04641
ACS Omega 2023, 8, 38301−38312

$$w_l^{(m)}(t) = \frac{2m+1}{\Delta z_l}\int_{\Omega_l} w_a(t,z)\phi_m(z)\mathrm{d}z,$$
$$g_l^{(m)}(t) = \frac{2m+1}{\Delta z_l}\int_{\Omega_l} g_a(C_a)\phi_m(z)\mathrm{d}z \quad (17)$$

The test function $\phi_m \in P^p(\Omega_l)$ will be used in place of the smooth function $v(z)$ and w and g the exact solutions are replaced by the approximate solution w_a and g_a. Also, the function $f(C_{l+1/2}, g_{l+1/2})$ is not defined at cell interfaces so it must be measured using an accurate numerical flux function H_l that considers the two values of $C_a(t, z)$ at the discontinuity, that is

$$f\left(C_{l+\frac{1}{2}}, g_{l+\frac{1}{2}}\right) \approx H_{l+\frac{1}{2}} = H\left(C^-_{l+\frac{1}{2}}, C^+_{l-\frac{1}{2}}\right) \quad (18)$$

where

$$C^-_{l+\frac{1}{2}} = \sum_{m=0}^{p} C_l^{(m)}\phi_m\left(z_{l+\frac{1}{2}}\right),$$
$$C^+_{l-\frac{1}{2}} = \sum_{m=0}^{p} C_l^{(m)}\phi_m\left(z_{l-\frac{1}{2}}\right) \quad (19)$$

Using the above definitions, the eqs 12 and 13 simplify to

$$\frac{\mathrm{d}w_l^{(m)}(t)}{\mathrm{d}t} = -\frac{2m+1}{\Delta z_l}\left(H_{l+\frac{1}{2}}\phi_m\left(z_{l+\frac{1}{2}}\right)H_{l-\frac{1}{2}}\phi_m\left(z_{l-\frac{1}{2}}\right)\right) + \frac{2m+1}{\Delta z_l}\int_{\Omega_l}\left(f(C_a, g_a)\frac{\mathrm{d}\phi_m(z)}{\mathrm{d}z}\right)\mathrm{d}z \quad (20)$$

$$g_l^{(m)}(t) = \frac{2m+1}{\Delta z_l}\sqrt{D_{app}}\left(C_{l+\frac{1}{2}}\phi_m\left(z_{l+\frac{1}{2}}\right) - C_{l-\frac{1}{2}}\phi_m\left(z_{l-\frac{1}{2}}\right) - \int_{\Omega_l} C_a(t,z)\frac{\mathrm{d}\phi_m(z)}{\mathrm{d}z}\mathrm{d}z\right) \quad (21)$$

Equation 20 gives the modified values of $w_l{=}C_l(t) + F^*_{q_l}(t)$ in each mesh interval Ω_l. In eq 20, the chain rule is used, and the system of ordinary differential equations in terms of C_l is obtained. Then, eqs 20 and 21 take the following form

$$\frac{\mathrm{d}C_l^{(m)}(t)}{\mathrm{d}t} = -\left(1 + F\left(\frac{\mathrm{d}q^*}{\mathrm{d}C}\right)_l^{(m)}\right)^{-1}\frac{2m+1}{\Delta z_l}\left(H_{l+\frac{1}{2}}\phi_m\left(z_{l+\frac{1}{2}}\right) - H_{l-\frac{1}{2}}\phi_m\left(z_{l-\frac{1}{2}}\right)\right) + \left(1 + F\left(\frac{\mathrm{d}q^*}{\mathrm{d}C}\right)_l^{(m)}\right)^{-1}\frac{2m+1}{\Delta z_l}\int_{\Omega_l}\left(f(C_a, g_a)\frac{\mathrm{d}\phi_m(z)}{\mathrm{d}z}\right)\mathrm{d}z \quad (22)$$

$$g_l^{(m)}(t) = \frac{2m+1}{\Delta z_l}\sqrt{D_{app}}\left(C_{l+\frac{1}{2}}\phi_m\left(z_{l+\frac{1}{2}}\right) - C_{l-\frac{1}{2}}\phi_m\left(z_{l-\frac{1}{2}}\right) - \int_{\Omega_l} C_a(t,z)\frac{\mathrm{d}\phi_m(z)}{\mathrm{d}z}\mathrm{d}z\right) \quad (23)$$

The initial data for the above system of differential equations are

$$C_l^{(m)}(0) = \frac{2m+1}{\Delta z_l}\int_{\Omega_l} C(0,z)\phi_m(z)\mathrm{d}z \quad (24)$$

$$g_l^{(m)}(0) = g(C_l^{(m)}(0)) \quad (25)$$

Boundary Conditions. The boundary was set at $z_{-1/2} = 0$. The left BC presented in eqs 4 and 5 can be applied as

$$C^-_{\frac{1}{2}}(t) = C_0^{(0)} + \frac{D_{app}}{u}\frac{C_1^{(0)} - C_0^{(0)}}{\Delta z} \quad (26)$$

$C_{N+1}^{(m)} = C_N^{(m)}$ is the outflow BC applied at the right end of the column.

Numerical Fluxes. Numerical fluxes are used to approximate the flow of information across discrete interfaces in a computational grid, which is then used to update the solution of the PDEs at each time step.[17−20,22,27−32] The choice of numerical fluxes is crucial and depends on the type of PDE being solved, the properties of the solution, and the desired accuracy of the solution. In order for the current numerical scheme to function effectively, it is required to select an accurate numerical flux function H_l to measure the cell interface flux values.[12] By defining a suitable numerical flux function that is consistent [i.e., $H_l(C_l, C_l) = F_l(C_l)$], monotone [i.e., $H_l(\cdot,\cdot)$ should be nondecreasing in its first argument and nonincreasing in its second argument], and Lipschitz continuous (i.e., there exists a Lipschitz constant $L > 0$ such that the absolute difference between the numerical flux function's values for different pairs of inputs should not be greater than L times the sum of the absolute differences in each input variable) accurate numerical results can be obtained.[34] A number of numerical flux functions have been documented in the literature.[38,39] Numerical fluxes play a key role in ensuring the stability and accuracy of numerical solutions, and their choice and implementation can greatly impact the performance and reliability of numerical simulations. Here, the local Lax−Friedrich flux function is utilized for this purpose[42]

$$H_l^{LLF}(c,d) = \frac{1}{2}[f_l(c, g_l(c)) + f_l(d, g_l(d)) - D(d-c)]$$

where

$$D = \max_{\min(c,d)\le s\le\max(c,d)} |f_l'(s, g_l(s))| \quad (27)$$

The scheme's total variation stability can be attained through modification of $C^{\pm}_{l\pm1/2}$ by utilizing a local projection limiter.[12,34] Thus

$$\tilde{C}_{l-\frac{1}{2}} = C_l^{(0)} - \tilde{C}_l, \qquad \tilde{\tilde{C}}_{l+\frac{1}{2}} = C_l^{(0)} + \tilde{\tilde{C}}_l \quad (28)$$

where

$$\tilde{C}_l = \sum_{m=1}^{M} C_l^{(m)}\phi_m\left(x_{l+\frac{1}{2}}\right),$$
$$\tilde{\tilde{C}}_{l,k} = -\sum_{m=1}^{M} C_l^{(m)}\phi_m\left(x_{l-\frac{1}{2}}\right) \quad (29)$$

Our work focuses on variation-bound approximations and the avoidance of negative values, particularly in chromatographic environments with strong gradients. We utilize linear basis functions ($M = 1$), as linear basis functions are

https://doi.org/10.1021/acsomega.3c04641
ACS Omega 2023, 8, 38301−38312

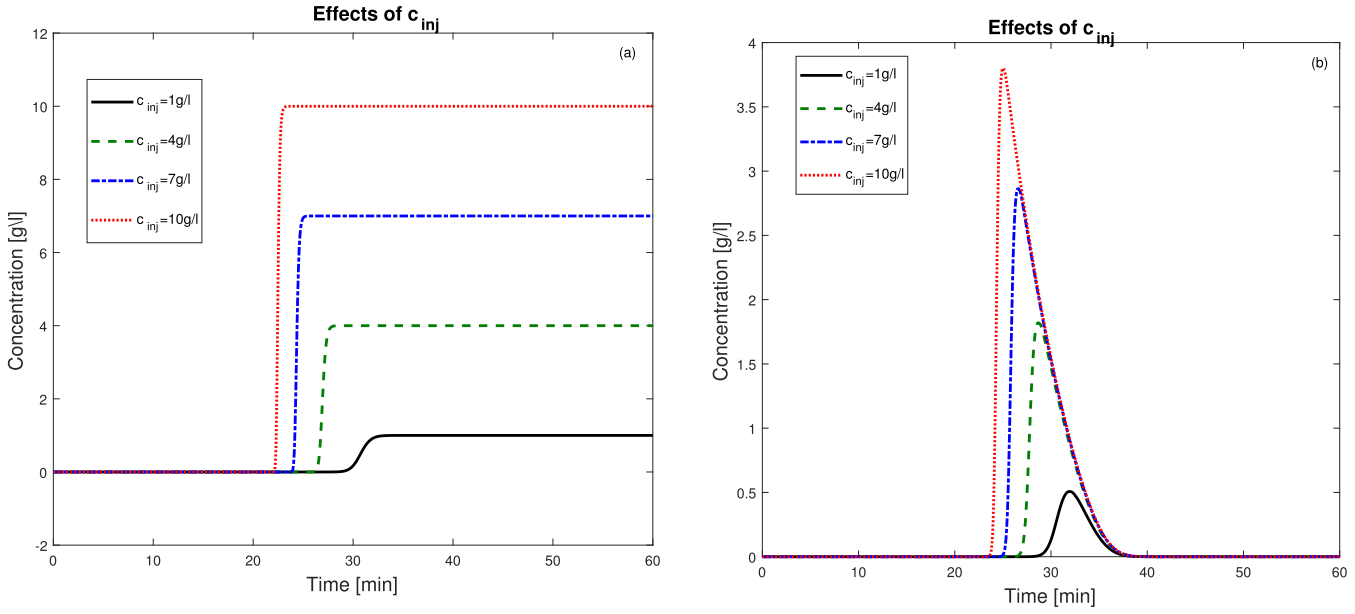

Figure 1. Effects of injected concentration in (a,b).

comparatively straightforward and simple to use in both their conceptual and computational aspects. Compared with higher-order basis functions, they use lower-order polynomials, which produce simpler expressions. By using linear basis functions with limiters, we are able to attain second-order accuracy, ensuring that the results of our calculations and simulations are highly precise and reliable.

To guarantee local positivity, the equations presented in eq 29 are updated through the implementation of van Leer slope limiters, as outlined in the studies of Jiang and Johnson.[40,41] When dealing with issues involving steep gradients, shocks, or discontinuities, we can improve the accuracy, stability, and physical relevance of numerical solutions by utilizing the limiters. As we are interested in variation-bounded approximations, these limiters are employed to maintain the non-negative nature of the expressions, ensuring that the results of our calculations remain physically meaningful as expressed below

$$\tilde{C}_l = mm(\tilde{C}_l,\ \Delta_+ C_l^{(0)},\ \Delta_+ C_l^{(0)}),$$
$$\tilde{\tilde{C}}_l = mm(\tilde{\tilde{C}}_l,\ \Delta_+ C_l^{(0)},\ \Delta_+ C_l^{(0)}) \tag{30}$$

The minmod function mm is defined as follows

$$mm(v_1, v_2, v_3) = \begin{cases} s\cdot \min\limits_{1\le j\le 3} |v_j|, & \text{if } \operatorname{sign}(v_1) = \operatorname{sign}(v_2) \\ & \quad = \operatorname{sign}(v_3) \\ & \quad = s \\ 0, & \text{otherwise} \end{cases} \tag{31}$$

Equation 28 can be written as

$$\tilde{C}_{l-\frac{1}{2}}^{(\mathrm{mod})} = C_l^{(0)} - \tilde{C}_l, \qquad \tilde{\tilde{C}}_{l+\frac{1}{2}}^{(\mathrm{mod})} = C_l^{(0)} + \tilde{\tilde{C}}_l \tag{32}$$

and eq 18 is modified as

$$H_{l+\frac{1}{2}} = H\left(\bar{C}_{l+\frac{1}{2}}^{(\mathrm{mod})},\ \bar{C}_{l-\frac{1}{2}}^{+(\mathrm{mod})}\right) \tag{33}$$

The local projection limiter established in eqs 30−32 ensures the scheme's stability while preserving its accuracy order. Controlling the magnitude of the solution in each computational cell helps prevent numerical errors and instability.[34] Additionally, the limiter is designed to preserve the order of accuracy, ensuring that the accuracy of the solution is not compromised. The local Lax−Friedrich numerical flux is utilized for the proposed model due to its simplicity, stability, and relatively high accuracy. The integral terms in eqs 20 and 23 are approximated by using the Gauss−Lobatto quadrature rule of order 10 which uses polynomial approximations to estimate the integrals. The implementation of the DG method yields a system of ODEs, as stated in eqs 22 and 23, as given below

$$\frac{\mathrm{d}\mathbf{w}_\mathrm{H}}{\mathrm{d}t} = L_\mathrm{H}(t, \mathbf{w}_\mathrm{H}) \tag{34}$$

where $\mathbf{w}_\mathrm{H} = [C_1, C_2, q_1, q_2]^T$. The system of ODEs mentioned above is solved using the rth-order TVB-RK method, as follows

$$\mathbf{w}_\mathrm{H}^{(i)} = \sum_{m=0}^{i-1} \{\alpha_{im}\mathbf{w}_\mathrm{H}^{(m)} + \gamma_{im}\Delta t L_\mathrm{H}(\mathbf{w}_\mathrm{H}^{(m)}, t^n + d_m\Delta t)\},$$
$$i = 1,2, \ldots, r \tag{35}$$

where the initial data are expressed as

$$\mathbf{w}_\mathrm{H}^{(0)} = \mathbf{w}_\mathrm{H}^n, \qquad \mathbf{w}_\mathrm{H}^{(r)} = \mathbf{w}_\mathrm{H}^{n+1} \tag{36}$$

where α_{km} and γ_{km} are the parameters of the TVB-RK method, n represents the time step monitor, and $\mathbf{w}_\mathrm{H}^{n+1}$ represents the solution at the next time step. The TVB-RK method parameters for a second-order scheme are written as[12]

$$\alpha_{10} = \gamma_{10} = 1, \qquad \alpha_{20} = \alpha_{21} = \gamma_{21} = \frac{1}{2},$$
$$\gamma_{20} = d_0 = 0, \qquad d_1 = 1 \tag{37}$$

Also, for the third-order scheme, the coefficients are defined as follows

https://doi.org/10.1021/acsomega.3c04641
ACS Omega 2023, 8, 38301−38312

$$\alpha_{10} = \gamma_{10} = 1,\ \alpha_{20} = \frac{3}{4},\ \gamma_{20} = 0,\ \alpha_{21} = \gamma_{21} = \frac{1}{4},$$
$$\alpha_{30} = \frac{1}{3},\ \gamma_{30} = \alpha_{31} = \gamma_{31} = 0,\ \alpha_{32} = \gamma_{32} = \frac{2}{3},$$
$$d_0 = 0,\ d_1 = 1,\ d_2 = \frac{1}{2} \tag{38}$$

RESULTS AND DISCUSSION

The suggested method is used to generate different chromatographic elutions. Numerical case studies for (i) a single-component one-dimensional ED model, (ii) a two-component one-dimensional ED model, and (iii) a three-component one-dimensional ED model are discussed.

Table 1. Basic Simulation Parameters of Single-Component Elution

parameters	symbols	values
column length	L	1 cm
dispersion coefficient	D_{app}	0.0001 cm^2/min
porosity	ϵ	0.4
interstitial velocity	u	0.1 cm/min
injection time	t_{inj}	2 min
maximum simulation time	t_{max}	60 min
initial concentration	C_{init}	0 g/L
feed concentration	C_{inj}	10 g/L
Henry constant for site I	a_{1I}	0.5
Henry constant for site II	a_{1II}	1.0
adsorption energy for site I	b_{1I}	0.05
adsorption energy for site II	b_{1II}	0.1

Elution Profile of One Component. In this subsection, we considered the nonlinear single-component ED model given by eq 6 along with the standard bi-Langmuir isotherm $q^*(C) = \frac{a_{1I}C}{1+b_{1I}C} + \frac{a_{1II}C}{1+b_{1II}C}$ (c.f. eq 2 with $p_j = 1$). Continuous injections in Figure 1a and rectangular injections in Figure 1b are both considered. The Danckwerts BCs given in eqs 3 and 4 are used. The required parameters used in this case study are given in Table 1.

Effects of Injected Concentration. Graphical results in Figure 1 show the impacts of the finite injected concentration on the profiles. Different injected concentrations, such as C_{inj} = 1 g/L, C_{inj} = 4 g/L, C_{inj} = 7 g/L, and C_{inj} = 10 g/L, are considered. The mixture pulse is injected into the column for t_{inj} = 12 min. In the figures, the peak height increased by increasing the injecting concentration. This demonstrates a direct correlation between the injection concentration and the height of the peaks.

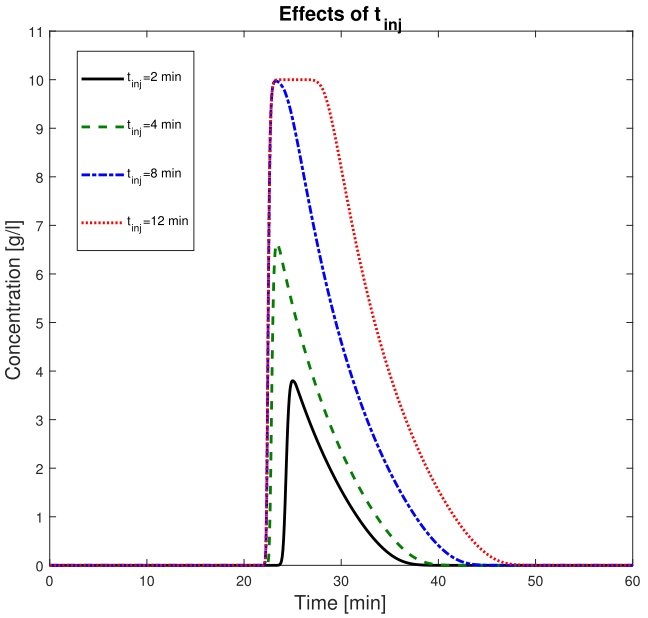

Figure 3. Effects of injection time t_{inj} on nonlinear single-component elution profile.

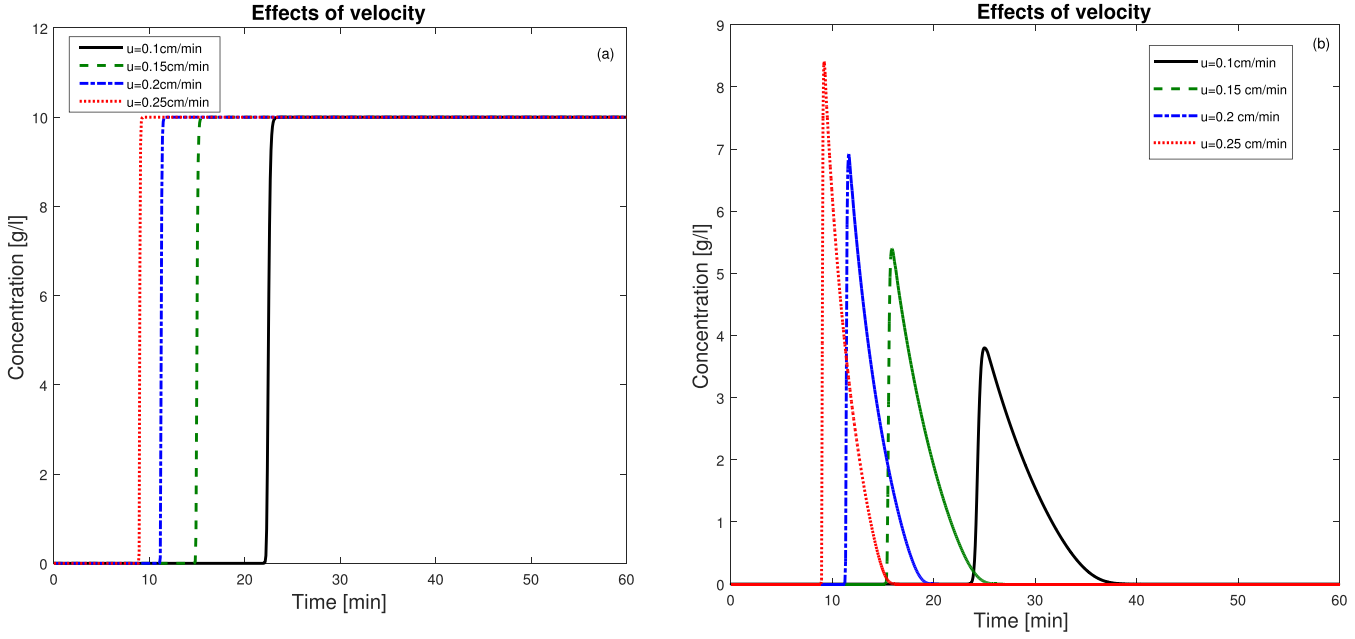

Figure 2. Effects of different velocities in (a,b).

https://doi.org/10.1021/acsomega.3c04641
ACS Omega 2023, 8, 38301−38312

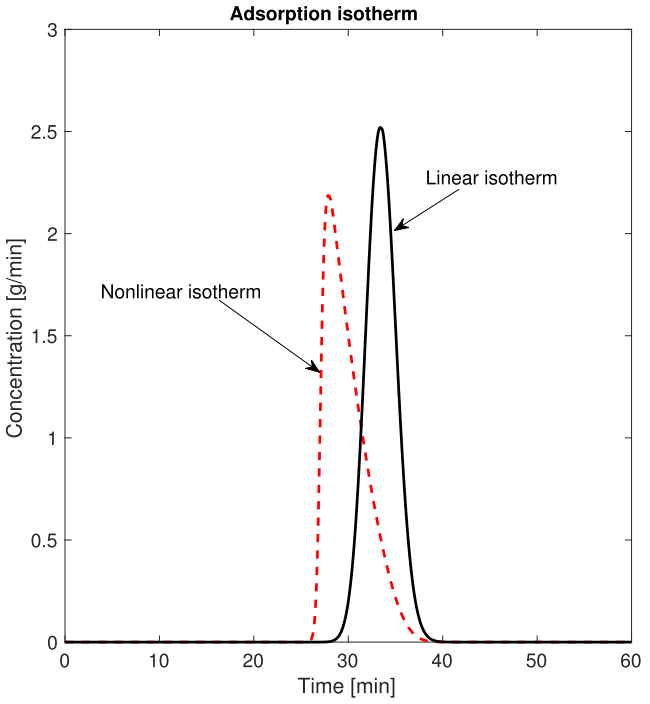

Figure 4. Effects of the adsorption isotherms.

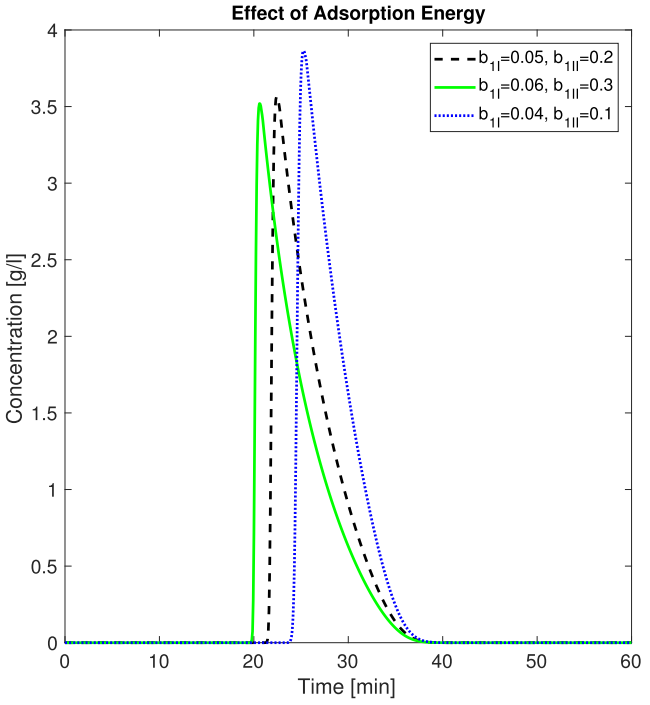

Figure 5. Effects of the adsorption energy.

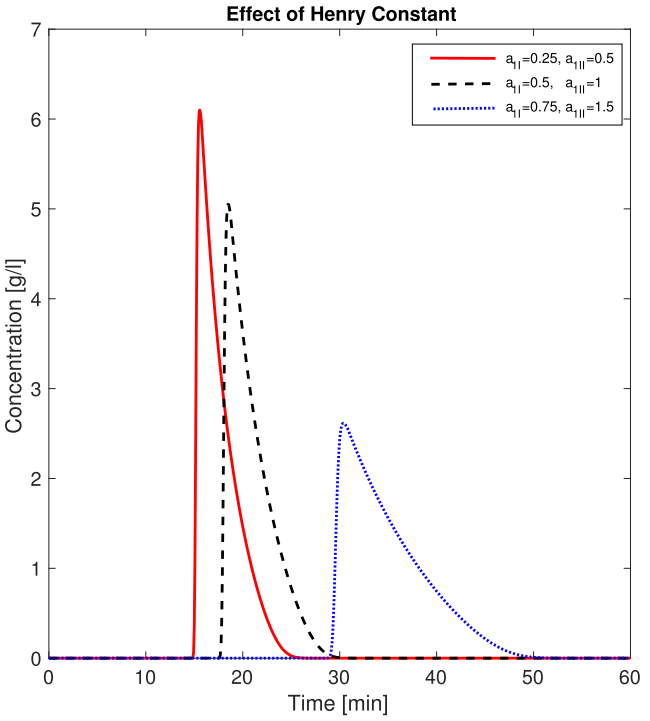

Figure 6. Effects of the Henry constant.

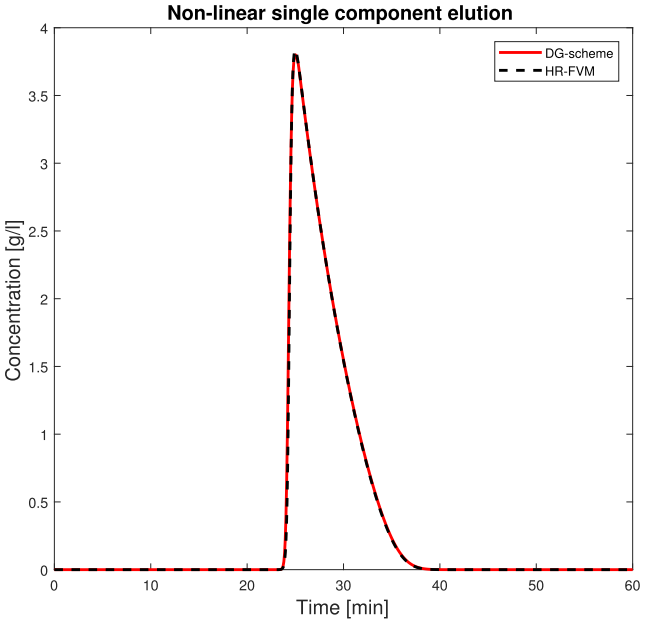

Figure 7. Comparison of the DG and FVM schemes.

Effects of Velocity. To investigate the effect of flow rate on retention time, concentration profiles were compared for both continuous and rectangular injections as in Figure 2a,b. Figure 2 shows the comparison for four different flow rates: u = 0.1, 0.15, 0.2, and 0.25 cm/min, while keeping the injection time constant at t_{inj} = 2 min. It was observed that the interstitial velocity had a significant impact on the retention time, with higher velocities leading to a decrease in the retention time. This effect is due to the dominant influence of adsorption at higher velocities. Consequently, the substance profiles in the system become more defined and pronounced.

Effects of Injected Time. The effects of the injection time on the concentration profile are shown in Figure 3. Four different values of injection time such as t_{inj} = 2 min, t_{inj} = 4 min, t_{inj} = 6 min, and t_{inj} = 12 min, respectively are considered for the injected concentration volume C_{inj} = 10 g/L. The plots depict that the increase in injection time increases the sample volume i.e., the width of rectangular profiles becomes wider. Furthermore, the effects of injected time are also visible from the right tail of the concentration profiles; therefore, its plot is

https://doi.org/10.1021/acsomega.3c04641
ACS Omega 2023, 8, 38301−38312

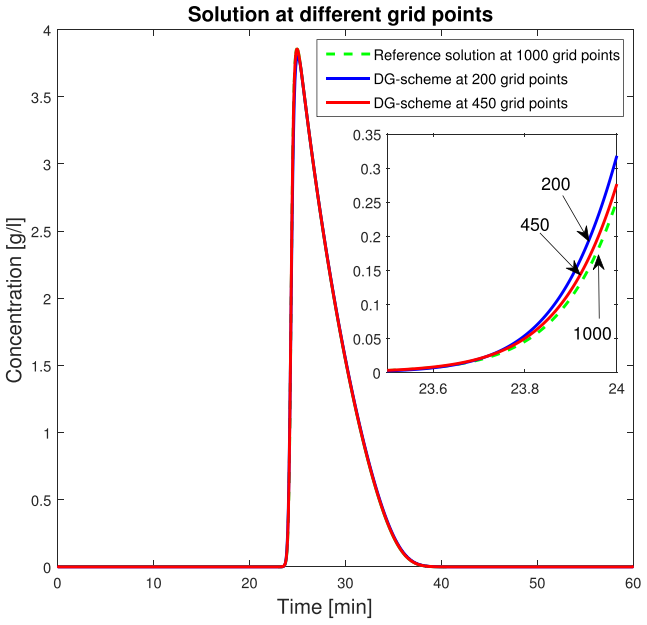

Figure 8. Solution at different grid points.

Table 2. Basic Simulation Parameters of Two-Component Elution

parameters	symbols	values
column Length	L	1.0 cm
dispersion coefficient	D_{app}	10^{-6} cm^2/min
porosity	ϵ	0.4
interstitial velocity	u	0.1 cm/min
injection time	t_{inj}	2.0 min
maximum simulation time	t_{max}	70 min
Henry constant for site I of comp. 1	a_{1I}	0.5
Henry constant for site II of comp. 1	a_{1II}	0.75
Henry constant for site I of comp. 2	a_{2I}	0.7
Henry constant for site II of comp. 2	a_{2II}	1.0
adsorption energy of comp. 1 for site I	b_{1I}	0.01
adsorption energy of comp. 1 for site II	b_{1II}	0.5
adsorption energy of comp. 2 for site I	b_{2I}	0.02
adsorption energy of comp. 2 for site II	b_{2II}	0.6

only possible for pulse injection because there is no tail in continuous injection.

Effects of Linear and Nonlinear Adsorption Isotherms. The impact of linear and nonlinear isotherms on the elution profile is given in Figure 4. The black solid line shows the linear isotherm, and the red dotted line shows the nonlinear isotherm. Normally, distributed peaks and symmetrical behavior are prominent in linear isotherm, whereas sharpening peaks, asymmetrical, and right tail behavior show the nonlinear isotherm effects. Decrease in the height and less retention time of the profiles are prominent in the case of nonlinear isotherm.

Effects of Adsorption Energy. In Figure 5 impact of the adsorption parameter is considered. For larger values of coefficients, decreases in the height and less retention time are prominent, which is due to the overloaded stationary phase as compared to smaller values of adsorption energies. Also, the right-tailed pattern of the bi-Langmuir isotherm is shown for a greater value of these coefficients.

Effects of Henry Constant. Figure 6 shows the effects of the Henry constant on the elution profile. It is used to predict the distribution of a substance between two phases. A higher value of the constant increases the retention time and decreases the height of the peak. This effect shows that the solubility rises for the smaller value of Henry's constant. Understanding the Henry constant is essential for optimizing the conditions in a system and achieving high-quality separations. In Figure 7, the already available high-resolution FVM of Koren[21,44] of second- to third-order accuracy is used to compare the results of the suggested method. The findings show an amazing level of accuracy and consistency.

Solution at Different Grid Points. In Figure 8, the effectiveness of the proposed scheme is examined over a grid of 200 and 450 mesh cells with a reference solution, whereas the reference solution is obtained by using RKDG over a grid of 1000 mesh cells. Comparing the results of the RKDG scheme on these different grid mesh cells with the reference solution aims to demonstrate how well the RKDG scheme converges to the reference solution as the grid is refined. In Figure 8, a clear comparison is evident as the grid is refined and the plot is close to the reference solution. This comparison provides valuable insights into the accuracy and reliability of the RKDG scheme in capturing the behavior of the reference solution, and validating its convergence properties.

Elution Profile of Two Components. We have stretched out our investigation to a nonlinear elution profile of two components. The numerical outcomes in these test problems are obtained by solving a two-component ED model by using the RKDG scheme with the Danckwerts BCs for unbounded and limited injected volumes.

Case 1: Generalized Bi-Langmuir Isotherm. To simulate how a two-component mixture will spread through a chromatographic column, we used the ED model eq 1 in conjunction with the standard bi-Langmuir isotherm eq 2, where we set $p_1 = -1$ and $p_2 = 1$.[24,25] All of the required parameters are given for the considered simulations in Table 2.

In accordance with a specific initial composition, the column is placed in a constant initial state. At time $\tau = 0$ a particular feed composition is continuously pumped into the column to produce an inlet state. This configuration corresponds to a particular Riemann problem for a small axial dispersion coefficient. The Riemann problem solutions are divided into three distinct elution fronts in the nonlinear chromatographic theory. Semishock waves, shock waves, and simple rarefaction waves are the characteristics of these elution fronts. In the equilibrium theory of nonlinear chromatography, shock is referred to as a mathematical discontinuity. Shock waves form when composition fronts in the upstream state move more quickly than those in the downstream state. This compression causes the shock waves to have a sharp front and improves the component concentration throughout the shock. Rarefaction waves are expansion waves by which the concentration decreases. As the mobile phase moves through the column, it can cause strong retention of a component, leading to the emergence of composition fronts. As the mobile phase moves through the column, it can cause strong retention of a component, leading to the emergence of composition fronts.

Simulation 1 of Case 1. The following data are utilized to run simulation 1 for case 1 as per our suggested numerical scheme. The constant initial concentrations and the feed concentrations are listed as $C_{1,init} = 0.0338$ g/L, $C_{2,init} = 0.262$ g/L, $C_{1,inj} = 0.4211$ g/L, and $C_{2,inj} = 0.0058$ g/L, for 1 and 2 component, respectively. The numerical results are shown in Figure 9 (left). Furthermore, in Figure 9 (right), comparisons

https://doi.org/10.1021/acsomega.3c04641
ACS Omega 2023, 8, 38301−38312

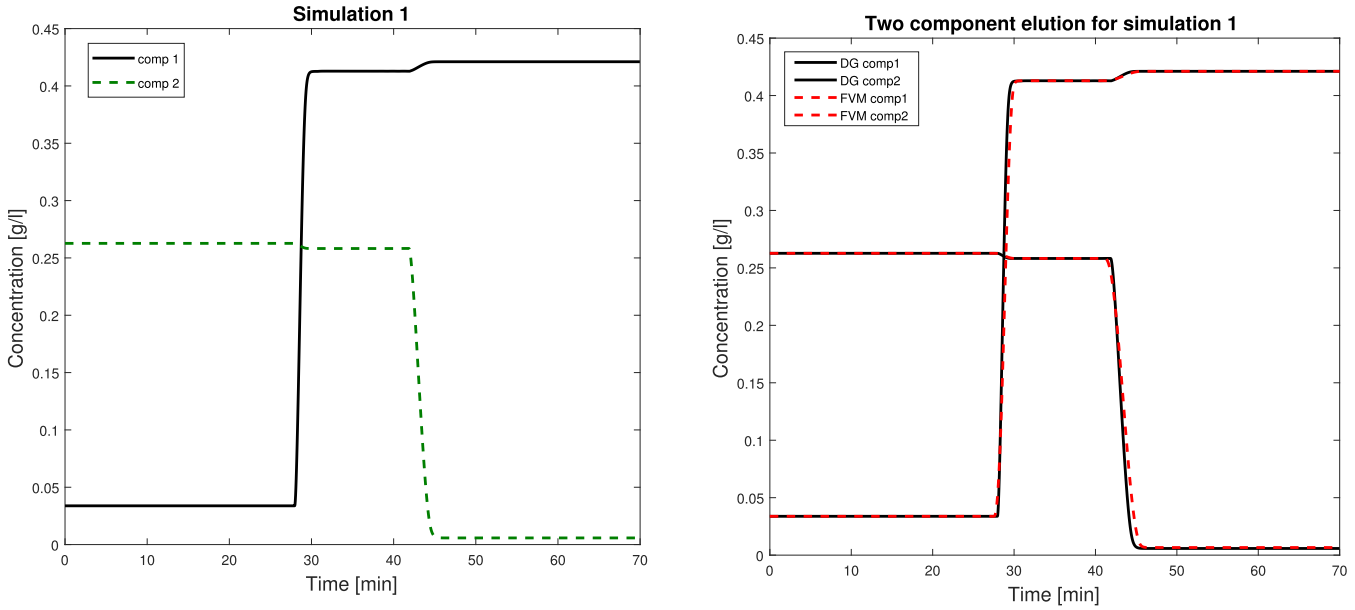

Figure 9. Simulation and comparison of schemes for case 1.

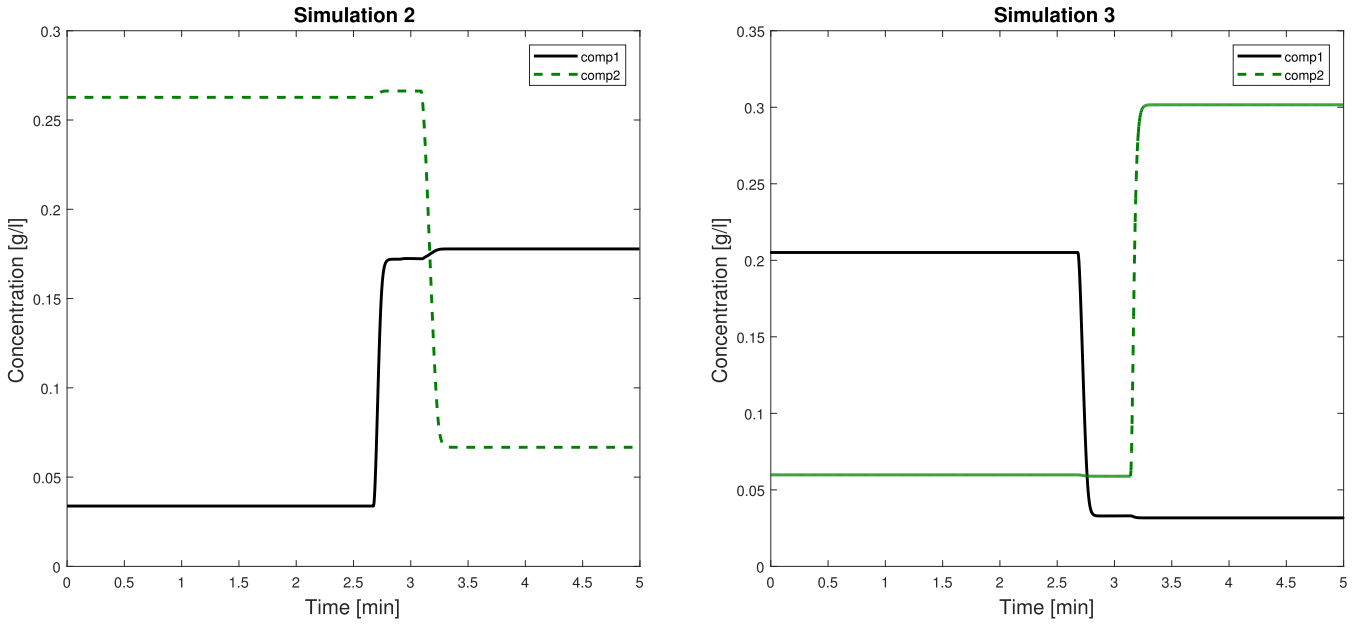

Figure 10. Simulations 2 and 3 for case 1.

of the RKDG and FVM methods are shown; both schemes produced similar results but the RKDG plots are slightly sharper than FVM.

Simulations 2 and 3 of Case 1. The following data are utilized to run simulations 2 and 3 for case 1 as per our suggested numerical scheme. The constant initial concentrations and the feed concentrations for simulation 2 are listed as $C_{1,\text{init}} = 0.0338$ g/L, $C_{2,\text{init}} = 0.262$ g/L, $C_{1,\text{inj}} = 0.1778$ g/L, and $C_{2,\text{inj}} = 0.0667$ g/L, for 1 and 2 component respectively, and the numerical results are presented in Figure 10 (left). Similarly, the constant initial concentrations and the feed concentrations for simulation 3 are listed as $C_{1,\text{init}} = 0.2051$ g/L, $C_{2,\text{init}} = 0.0598$ g/L, $C_{1,\text{inj}} = 0.0317$ g/L, and $C_{2,\text{inj}} = 0.3016$ g/L, for 1 and 2 component respectively, and the numerical results are shown in Figure 10 (right).

Case 2: Standard Bi-Langmuir Isotherm. For finite injected volumes, two-component ED [c.f. eq 1 with standard bi-Langmuir isotherm given in eq 2 with $(p_1 = 1 \ \& \ p_2 = 1)$] is considered. All of the required parameters needed for this test problem are given in Table 2. At the column inlet, a liquid mixture is injected for $t_{\text{inj}} = 12$ min to produce the numerical result presented in Figure 11.

Effects of High Values of Adsorption Energy. In Figure 12, the effects of high values of adsorption energy are considered. The overlapping in the concentration profiles shows poor separation, and accurately identifying and quantifying individual components might be difficult when there are overlapping peaks. It also increases the retention time as analytes interact with the stationary phase for a longer period of time before eluting from the column.

https://doi.org/10.1021/acsomega.3c04641
ACS Omega 2023, 8, 38301−38312

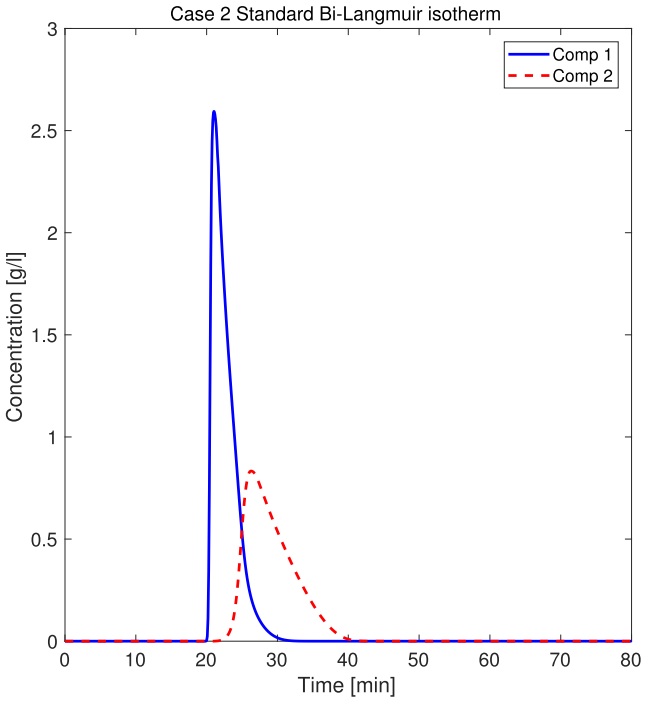

Figure 11. Elution profile for two components.

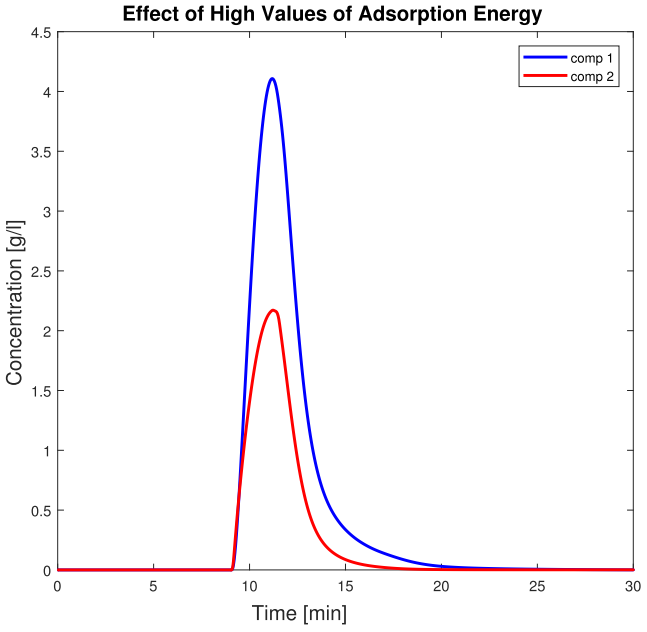

Figure 12. Effects of high adsorption energy.

Elution Profile of Three Components. Figure 13 displays the three-component elution profiles of the mixture. The following data values are used in the simulation process $\epsilon = 0.4$, $L = 1$ cm, $u = 0.1$ cm/min, $a_{1I} = 1.0$, $a_{1II} = 0.75$, $a_{2I} = 0.5$, $a_{2II} = 2.0$, $a_{3I} = 0.25$, $a_{3II} = 3.5$, $b_{1I} = 0.05$, $b_{1II} = 0.015$, $b_{2I} = 0.0001$, $b_{2II} = 0.1$, $b_{3I} = 0.02$, $b_{3II} = 1.0$, $D_z = 0.0001$ cm^2/min, $C_{k,inj} = 1$ g/L, and $t_{max} = 100$ min. The standard bi-Langmuir isotherm is used in eq 2. At first, an empty column is taken i.e., $c_{k,init} = 0$ g/L. The typical behavior of the bi-Langmuir adsorption isotherm is visible from the results shown in Figure 13. Adsorption equilibrium constants components with higher values eluted from the column later than those with smaller values.

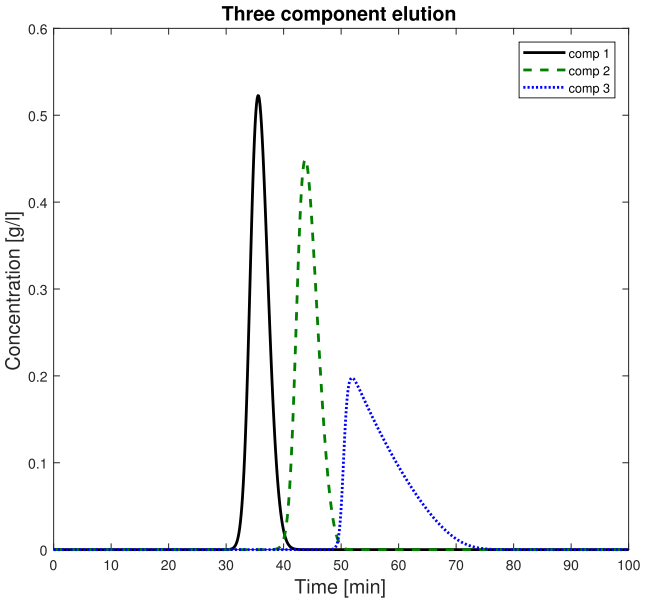

Figure 13. Elution profile for three components.

CONCLUSIONS

In this paper, a multicomponent nonlinear ED model was formulated and solved numerically. The ED model was then solved by using the TVB-RKDG method. First, the system of ODEs was created from the given PDE by using the DG method in the axial coordinate, and then an explicit and nonlinearly stable high-order Runge−Kutta method, i.e., TVB-RK, was used to solve the resulting ODE system. The TVB property ensures the scheme's positivity, such as in this work the non-negativity of the mixture concentrations. Numerous case studies involving one, two, and three components were used to examine the model. The effects of different kinetic parameters such as the effects of injected concentration, velocity, linear and nonlinear isotherm, adsorption energies, Henry constant, and injected time are considered for the efficiency of the process. It helps us to examine the consequences of uncertainties in the inlet concentrations. All of the findings in this article were attained in a minute. The graphical comparison was shown for two numerical methods: the FVM and FEM. The proposed RKDG method ensures convergence to physically relevant solutions by achieving stable and nonoscillatory solutions and the TVB property ensures the scheme's positivity as it is the most prevalent and fundamental mathematical requirement in physical models. The utilization of these simulations has numerous benefits when it comes to improving the experimental setup and transport mechanisms. These simulations allow for the optimization of the experimental conditions by providing a virtual environment to test and fine-tune various parameters. The proposed scheme can also be applied to more complex geometries. Additionally, they are also useful in scaling up the physiochemical variables, which can be crucial in obtaining accurate results when transitioning from laboratory to industrial-scale processes. By incorporating these simulations into the experimental design process, we can achieve more efficient and effective results, leading to a greater understanding of the system being studied.

https://doi.org/10.1021/acsomega.3c04641
ACS Omega 2023, 8, 38301−38312

AUTHOR INFORMATION

Corresponding Author

Ambreen Khan − *Department of Mathematics, Air University, Islamabad 44000, Pakistan;* orcid.org/0009-0007-9221-6288; Email: ambreen.khan@mail.au.edu.pk

Author

Shamsul Qamar − *Department of Mathematics, COMSATS University Islamabad, Islamabad 45550, Pakistan;* orcid.org/0000-0002-7358-6669

Complete contact information is available at: https://pubs.acs.org/10.1021/acsomega.3c04641

Notes

The authors declare no competing financial interest.

ACKNOWLEDGMENTS

We appreciate the useful suggestions provided by the anonymous referees.

REFERENCES

(1) Guiochon, G. Preparative liquid chromatography. *J. Chromatogr. A* **2002**, *965*, 129−161.

(2) Guiochon, G.; Lin, B. *Modeling for Preparative Chromatography*; Academic Press, 2003.

(3) Guiochon, G.; Felinger, A.; Shirazi, D. G., Katti, A. M. *Fundamentals of Preparative and Nonlinear Chromatography*, 2nd ed.; ELsevier Academic press: New York, 2006.

(4) Ruthven, D. M. *Principles of Adsorption and Adsorption Processes*; Wiley-Interscience: New York, 1984.

(5) von Lieres, E.; Andersson, J. A Fast and accurate solver for the general rate model of column liquid chromatography. *Comput. Chem. Eng.* **2010**, *34*, 1180−1191.

(6) Reed, W. H.; Hill, T. R. *Triangular Mesh Methods for the Neutron Transport Equation (No. LA-UR-73-479; CONF-730414-2)*; Los Alamos Scientific Lab.: N. Mex. (USA), 1973.

(7) Lesaint, P.; Raviart, P. A. *On a Finite Element Method for Solving the Neutron Transport Equation*; Publications mathématiques et informatique de Rennes, 1974; pp 1−40.

(8) Javeed, S.; Qamar, S.; Seidel-Morgenstern, A.; Warnecke, G. Efficient and accurate numerical simulation of nonlinear chromatographic processes. *Comput. Chem. Eng.* **2011**, *35*, 2294−2305.

(9) Qamar, S.; Perveen, S.; Seidel-Morgenstern, A. Numerical approximation of nonlinear and non-equilibrium two-dimensional model of chromatography. *Comput. Chem. Eng.* **2016**, *94*, 411−427.

(10) Bassi, F.; Rebay, S. A high order accurate discontinuous finite element method for the numerical solution of the compressible Navier-Stokes equations. *J. Comput. Phys.* **1997**, *131*, 267−279.

(11) Qamar, S.; Abbasi, J. N.; Javeed, S.; Shah, M.; Khan, F. U.; Seidel-Morgenstern, A. Analytical solutions and moment analysis of chromatographic models for rectangular pulse injections. *J. Chromatogr. A* **2013**, *1315*, 92−106.

(12) Javeed, S.; Qamar, S.; Seidel-Morgenstern, A.; Warnecke, G. A discontinuous Galerkin method to solve chromatographic models. *J. Chromatogr. A* **2011**, *1218*, 7137−7146.

(13) Püttmann, A.; Nicolai, M.; Behr, M.; von Lieres, E. Stabilized space-time finite elements for high-definition simulation of packed bed chromatography. *Finite Elem. Anal. Des.* **2014**, *86*, 1−11.

(14) Püttmann, A.; Schnittert, S.; Leweke, S.; von Lieres, E. Utilizing algorithmic differentiation to efficiently compute chromatograms and parameter sensitivities. *Chem. Eng. Sci.* **2016**, *139*, 152−162.

(15) Qamar, S.; Sattar, F. A.; Abbasi, J. N.; Seidel-Morgenstern, A. Numerical simulation of nonlinear chromatography with core-shell particles applying the general rate model. *Chem. Eng. Sci.* **2016**, *147*, 54−64.

(16) Rouchon, P.; Schonauer, M.; Valentin, P.; Guiochon, G. Numerical Simulation of Band Propagation in Nonlinear Chromatography. *Sep. Sci. Technol.* **1987**, *22*, 1793−1833.

(17) Cruz, P.; Santos, J. C.; Magalhães, F.; Mendes, A. Simulation of separation processes using finite volume method. *Comput. Chem. Eng.* **2005**, *30*, 83−98.

(18) Webley, P. A.; He, J. Fast solution-adaptive finite volume method for PSA/VSA cycle simulation; 1 single step simulation. *Comput. Chem. Eng.* **2000**, *23*, 1701−1712.

(19) LeVeque, R. J. *Numerical Methods for Conservation Laws*; Birkhaüser Verlag: Bassel, Germany, 1992.

(20) Leer, B. V. Towards the ultimate conservative difference scheme. IV. A new approach to numerical convection. *J. Comput. Phys.* **1977**, *23*, 276−299.

(21) Koren, B.; A robust upwind discretization method for advection, diffusion and source terms. *Numerical Methods for Advection-Diffusion Problems: Vol. 45 of Notes on Numerical Fluid Mechanics*; Vreugdenhil, C. B., Koren, B., Eds.; Vieweg Verlag: Braunschweig, 1993; Chapter 5, pp 117−138.

(22) Gottlieb, S.; Shu, C.-W. Total Variation Diminishing Runge-Kutta Schemes. *Math. Comput.* **1998**, *67*, 73.

(23) Dondi, F.; Guiochon, G. *Theoretical Advancement in Chromatography and Related Separation Techniques*; Springer Science +Business Media: Dordrecht, Ferrara, Italy, 1992.

(24) Mazzotti, M. Local equilibrium theory for the binary chromatography of species subject to a generalized langmuir isotherm. *Ind. Eng. Chem. Res.* **2006**, *45* (15), 5332−5350.

(25) Mazzotti, M. Nonclassical composition fronts in nonlinear chromatography: Delta-shock. *Ind. Eng. Chem. Res.* **2009**, *48*, 7733−7752.

(26) Danckwerts, P. V. Continuous flow systems. *Chem. Eng. Sci.* **1953**, *2*, 1−13.

(27) Sweby, P. K. High resolution schemes using flux limiters for hyperbolic conservation laws. *SIAM J. Numer. Anal.* **1984**, *21*, 995−1011.

(28) Roe, P. L. Characteristic-based schemes for the Euler equations. *Annu. Rev. Fluid. Mech.* **1986**, *18*, 337−365.

(29) van Leer, B. Towards ultimate conservative finite difference scheme.2. Monotonicity and conservation combined in a second-order scheme. *J. Comput. Phys.* **1974**, *14*, 361−370.

(30) Kondrat, S.; Zimmermam, O.; Wiechert, W.; von-Lieres, E. Discrete-continuous reaction-diffusion model with mobilepoint-like sources and sinks. *Eur. Phys. J. E* **2016**, *39*, 11.

(31) Leweke, S.; von-Lieres, E. Fast arbitrary order moments and arbitrary precision solution of the general rate model of column liquid chromatography with linear isotherm. *Comput. Chem. Eng.* **2016**, *84*, 350−362.

(32) Ghosh, P.; Vahedipour, K.; Leuthold, M.; von-Lieres, E. Model-based analysis and quantitative prediction of membrane chromatography: Extreme scale-up from 0.08 mL to 1200 mL. *J. Chromatogr. A* **2014**, *1332*, 8−13.

(33) Qiu, J. X.; Khoo, B. C.; Shu, C.-W. A numerical study for the performance of the Runge-Kutta discontinuous Galerkin method based on different numerical fluxes. *J. Comput. Phys.* **2006**, *212*, 540−565.

(34) Cockburn, B.; Shu, C.-W. TVB Runge-Kutta local projection discontinuous Galerkin finite element method for conservation laws II: General Framework. *Math. Comput.* **1989**, *52*, 411−435.

(35) Meyer, K.; Huusom, J. K.; Abildskov, J. High order approximation of chromatographic models using a nodal discontinuous Galerkin approach. *Comput. Chem. Eng.* **2018**, *109*, 68−76.

(36) Cockburn, B.; Hou, S.; Shu, C.-W. The Runge-Kutta local projection discontinuous Galerkin finite element method for conservation laws. IV. The multidimensional case. *Math. Comput.* **1990**, *54* (190), 545−581.

(37) Cockburn, B.; Shu, C.-W. The Runge-Kutta discontinuous Galerkin method for conservation laws V: multidimensional systems. *J. Comput. Phys.* **1998**, *141* (2), 199−224.

(38) Zhang, P.; Liu, R. X. Hyperbolic conservation laws with space-dependent fluxes: II. General study of numerical fluxes. *J. Comput. Appl. Math.* **2005**, *176* (1), 105−129.
(39) Kurganov, A.; Tadmor, E. New high resolution central schemes for nonlinear conservation laws and convection diffusion equations. *J. Comput. Phys.* **2000**, *160* (1), 241−282.
(40) Jiang, G. S.; Shu, C. W. On a cell entropy inequality for discontinuous Galerkin methods. *Math. Comput.* **1994**, *62* (206), 531−538.
(41) Johnson, C. Error estimates and adaptive time-step control for a class of one-step methods for stiff ordinary differential equations. *SIAM J. Numer. Anal.* **1988**, *25* (4), 908−926.
(42) Cockburn, B.; Shu, C. W. Runge Kutta discontinuous Galerkin methods for convection-dominated problems. *J. Sci. Comput.* **2001**, *16* (3), 173−261.
(43) Breuer, J. M.; Leweke, S.; Schmölder, J.; Gassner, G.; von Lieres, E. Spatial discontinuous Galerkin spectral element method for a family of chromatography models in CADET. *Comput. Chem. Eng.* **2023**, *177*, 108340.
(44) Khan, A.; Perveen, S.; Shaheen, Z.; Qamar, S. Numerical approximation of non-linear chromatographic models considering Bi-Langmuir isotherm. *Therm. Sci.* **2022**, *26*, 77−93.

https://doi.org/10.1021/acsomega.3c04641
ACS Omega 2023, 8, 38301−38312